



Convective instability with time scale translation of the transmitted fluctuation

Koichi Fujimoto* , Kunihiro Kaneko

*Department of Pure and Applied Sciences, Graduate School of Arts and Sciences, University of Tokyo,
3-8-1, Komaba, Meguro, Tokyo 153-8902, Japan*

Received 26 February 2004; received in revised form 28 April 2004; accepted 28 April 2004

Communicated by Y. Kuramoto

Abstract

Convective instability in an open flow system with distributed time scales from upstream to downstream is studied. By exploiting the convective instability, the upstream fluctuation with fast time scale is not only amplified along the flow but is also slowed down along the flow to the downstream. Through the instability, statistical property of the downstream shows sensitive dependence on the dynamics of the fast element in the upstream, and the fast dynamics is translated into slower dynamics. This convective instability and sensitive dependence on the boundary are analyzed, by noting the time scale multiplication of fluctuation with repetition of bifurcation through the transmission. Relevance of this process to biochemical reaction and memory is discussed. © 2004 Elsevier B.V. All rights reserved.

PACS: 05.40.+j; 05.45.-a; 47.70.Fw; 89.75.Fb

Keywords: Multiple time scales; Open flow; Convective instability; Noise-sustained structure; Time scale multiplication

1. Introduction

Many problems in physical, chemical, biological, and geo-physical systems involve multiple time scales [1–3]. In particular, in a cell system, fast change in the metabolic reactions can successively be embedded into the change of genetic level. Hierarchical organization of time scales ranging from subcellular to multicellular level is also experimentally studied [4]. Study of such dynamical systems with multiple time scales is also important to understand biological memory, where fast change in some degrees of freedom induced by the external input is successively embedded into downstream degrees of freedom and stored into the final internal states, which have a much longer time scale.

* Corresponding author.

E-mail address: fujimoto@complex.c.u.-tokyo.ac.jp.

In these problems, modes with highly different time scales interact with each other, which may introduce complex dynamics having a wide range of time scales. In general, study of dynamical organization of a system with many degrees of freedom and multiple time scales may provide a novel viewpoint to understand the hierarchical organization in nature [5]. As a step to these studies, we have taken dynamical systems with many degree of freedom [6] here.

In our previous study [10], we introduced a chain of nonlinear oscillators whose typical time scales are distributed as a power series. To be specific, we have chosen a nonlinear differential equation as the single oscillator, and introduced the difference in the time scale as

$$T_i \frac{d\vec{A}_i}{dt} = \vec{F}(\vec{A}_i), \quad T_i \equiv T_1 \tau^{i-1} \quad (1)$$

The index of the elements is denoted as i with $i = 1, 2, \dots, L = \text{system size}$. T_i is the characteristic time scale for each element and $\tau (>1)$ is the time scale difference. By using a power series distribution for the characteristic time scales, the relationship between any neighboring elements is identical, as is easily checked by scaling the time t by T_i in each equation for the element. Hence, this form is useful to study the relevance of time scale variation, since the dynamics of each element, after rescaling of the time, is identical. In the previous model, we adopted symmetric coupling between the nearest neighboring elements, and investigated how statistical (topological) properties of the slow dynamics are affected by those of the fast dynamics. In particular, bifurcation cascade between chaotic and regular dynamics is shown to lead to the propagation of correlation from fast to slow elements, with successive change of synchronization.

On the other hand, asymmetric coupling from upper flow to downflow is often important. In an intra-cellular signalling system, there is a cascade of the reaction that successively catalyzes the phosphorylation of a specific molecule species, such as MAP kinase cascade. Also, there is a flow from the cell membrane to the inside of a cell, reaching nucleus [11]. In brain, fast external changes are coupled to internal layers successively, leading to long-term memory, for example, long-term potentiation [12]. In these examples, the coupling is not symmetric, but highly asymmetric from the external signal to the most internal element. Often, with this directional coupling, fast external changes are successively transferred to slow internal changes. In other words, the direction of coupling is correlated with the change of the time scale in the dynamics. Hence, it is interesting to study a model with directional coupling together with the flow form of dynamics from upstream to downflow.

Understanding the above process is important for signal transduction in a cell. More generally speaking, it is relevant to study how a biological system embeds external information into its inside, a necessary condition for biological memory in general.

In a system with a directional coupling, fluctuations of the upstream can be amplified as they are propagated into the downflow. Such amplification along the flow is called convective instability, which is frequently observed in an open fluid flow system, and is an essential concept to discuss the propagation and amplification of the fluctuation [7–9]. The convective instability with time scale variation is observed in a surface flow of a sand-pile, as will be discussed again in Section 7.3.

In the present paper, we study the propagation of the correlation to slower elements, in connection with the convective instability, instead of the chaotic instability in the previous study. By introducing and investigating an open flow system whose time scale varies from the upstream to the downstream, we will report a new type of the convective instability that allows for the *time-scale transformation* of fluctuation. Through repetition of bifurcations from upstream to downstream, fast time scale motion is successively transformed to slower motions. This repetition of bifurcation is analogous to the cascade of the bifurcation in coupled chaotic elements with power law time scale variation as reviewed above [10].

The present paper is organized as follows. In Section 2, the concept of convective instability is briefly reviewed. In Section 3, we introduce an open-flow reaction chain model, with a unidirectional coupling. In addition, the time-scale of oscillation of each element changes with a power-series from fast (upstream) to slow (downstream) element, as a result of the concentration change of catalyst or molecule species characterizing the activity of the reaction.

In Section 4, we report the convective instability with the time scale translation. Here the transmitted fluctuation is not only amplified from the upstream to the downstream but also the time scale of the dynamics is made slower. In Section 5, we discuss the mechanism of the time scale multiplication. If the system is convectively unstable only within a range of frequency, the fluctuation only within a range is amplified as in a band pass filter. Furthermore, when the time scale multiplication of the fluctuation occurs repeatedly during the transmission from the upstream to the downstream, the time scale is translated through the propagation. In Section 6, we will show that *sensitive* dependence of the slow dynamics on the fast elements is resulted from the above instability. Section 7 is devoted to discussion and conclusion.

2. Convective instability

Convective instability causes amplification of a disturbance along a flow [7–9]. If a system is convectively unstable (CU), tiny disturbance at an upstream is amplified and transmitted as it goes to the downstream, as is originally discussed for the open fluid flow.

As a model for the open flow systems, coupled nonlinear oscillators with asymmetric coupling [13–16] and nonlinear partial differential equation with asymmetric diffusion [9,17] or advection [18,19] have been studied.

2.1. Noise-sustained structure

For a system with the convective instability, noise plays an important role. When a system is convectively unstable, applied noise at one point is spatially amplified to the downflow, until at some point, some spatiotemporal structure with a finite amplitude is generated accordingly. This structure is not generated without noise, and is called noise-sustained structure (NSS) [17].

The mechanism of the structure formation can be summarized as follows. Assume that noise is added to a fixed point state with convective instability. Around the fixed point, the noise is spatially amplified and transmitted to the downstream direction. The further the fluctuation is propagated to the downflow, the larger the oscillation becomes, until some stationary dynamics (such as oscillation with a large amplitude) is generated for a certain downflow region. As long as the noise is added to the most upstream element, this downstream dynamics are generated. This noise-induced structure in a convectively unstable system is general in an open-flow model. In contrast, if the fixed point state is absolutely stable (AS) at all positions, noise is spatially damped, and no downstream structure can be sustained.

2.2. Measure of convective instability

Convective instability is quantitatively characterized by a co-moving Lyapunov exponent λ_v , i.e., the Lyapunov exponent observed in an inertial system moving with a velocity v [20,21]. If $\max_v \lambda_v$ is positive for a given state, the state is convectively unstable. This condition is compared with that for the linear instability, given by $\lambda_0 > 0$. Absolute stability, which implies the stability along any flow [7,8], is guaranteed by the condition $\max_v \lambda_v < 0$. Since λ_v characterizes the amplification of a perturbation with the velocity v , the amplification per one spatial unit is given by λ_v/v . Hence, the amplification rate per length is given by the spatial Lyapunov exponent λ^S [22,23];¹

$$\lambda^S = \max_v \frac{\lambda_v}{v} \quad (2)$$

λ^S is also calculated by spatial amplification rate of the amplitude of the fluctuation along the flow, as will be adopted in Section 3.3.

¹ In intermittent systems, for example, with a large amplitude fluctuation, Eq. (2) is replaced by $\lambda^S \geq \max_v \lambda_v/v$ [23].

In the present paper, since we discuss the time scale translation of the transmitted fluctuation from the upstream to the downstream, it is also necessary to characterize the convective instability with regards to the frequency of perturbations. Here we adopt the degree of the convective instability to a periodic perturbation² with frequency f [24,25] as $\kappa(f)$, as is introduced in Appendix A.

3. Model

3.1. Reaction-flow equation as a model for open flow systems

To make an explicit example of the uni-directional coupling system, we first consider simple autocatalytic kinetics given by



The evolution equations for A, B are then written as

$$\begin{cases} \dot{a} = k_1 - ab^2 \\ \dot{b} = ab^2 - k_2b \end{cases} \quad (4)$$

where a, b are the concentration of A, B and k_1 and k_2 are rate constants of the reactions. We set $k_1 = 1.01, k_2 = 1.5$, so that $(a(t), b(t))$ converges to a linearly stable fixed point $(a_*, b_*) = (k_2^2/k_1, k_1/k_2)$. There is neither a stable limit cycle nor another stable fixed point, besides the above fixed point for any initial conditions.³

As a model for the open flow system with the convective instability, we choose a one-dimensional chain of the above reaction system with flow and diffusion equation as,

$$\begin{cases} \frac{\partial a}{\partial t} = k_1 - ab^2 \\ \frac{\partial b}{\partial t} = ab^2 - k_2b + v_g \frac{\partial b}{\partial x} + D_b \frac{\partial^2 b}{\partial x^2} \end{cases} \quad (5)$$

The model has been studied for oscillatory pattern induced by the convective instability [19].

In the present paper, we consider the open flow systems whose time scale spatially varies. Here we introduce the exponential time scale variation for Eq. (11) as

$$\begin{cases} \exp(k_x x) \frac{\partial a}{\partial t} = k_1 - ab^2 \\ \exp(k_x x) \frac{\partial b}{\partial t} = ab^2 - k_2b + v_g \frac{\partial b}{\partial x} + D_b \frac{\partial^2 b}{\partial x^2} \end{cases} \quad (6)$$

where k_x denotes the exponential time scale gradient in the reaction-diffusion system.

Since the flow term $\partial b/\partial x$ is essential for the convective instability and the diffusion term $\partial^2 b/\partial x^2$ is qualitatively irrelevant to the results described below, the diffusion term is eliminated in the present paper for the simplicity of the analysis. Also for the simplicity, the upwind differencing⁴ is adopted. Accordingly, we study a system of

² Dependence of the periodicity on the boundary condition has been studied numerically [16] and experimentally [26]. There, the generated state and the degree of the convective instability at the downstream are dependent on the period.

³ The model is essentially same as Brusselator model [27], one of the most studied nonlinear dynamics. We adopt this particular model as a typical example. The results to be shown generally hold for a coupled chain of the oscillators (with amplitude and phase), and the details of the model are not important.

⁴ Spatial discretization using the upwind differencing is one of the simplest way to model the transport properties [30]. It is also qualitatively irrelevant to our results.

unidirectionally coupled nonlinear oscillators as

$$\begin{cases} T_i \dot{a}_i = k_1 - a_i b_i^2 \\ T_i \dot{b}_i = a_i b_i^2 - k_2 b_i + v(b_{i-1} - b_i) \end{cases} \quad (7)$$

with

$$\begin{cases} T_i \equiv \tau^i \\ \tau \equiv \exp(k_x) \end{cases} \quad (8)$$

where $v = v_g/\delta x$ with δx as the length between the neighboring sites, T_i is characteristic time scale of each element, $T_1 = 1$, and $\tau (>1)$ is time scale difference per element. The index i denotes each element, $i = 1, 2, \dots, L =$ systemsize. The power series distribution of the characteristic scales is common to Eq. (1). Again, the relationship between the neighboring elements is identical. The boundary condition b_0 is fixed to the value as same as the fixed point $b_0 = b_*$ in Eq. (4).

The total time scale difference is given by

$$T_{\text{total}} \equiv \frac{T_L}{T_1} = \tau^{L-1} \quad (9)$$

Here we set $T_{\text{total}} = 100$, and adopt Runge–Kutta method using such time step size that the fastest element \vec{A}_i at $i = 1$ is computed precisely.

3.2. Construction of the open flow with time scale variation

In this subsection, we discuss origins of the time scale variation in the spatially extended system as assumed in the model Eq. (6), (Eq. 7)).

One source of such time scale variation is observed in soft materials, for example, in granular matter. In the avalanche behavior of a sand pile, it is observed that the particle flow on the surface is faster, and the velocity gets slower as the position of the particle goes farther away from the surface [31], in strong contrast with the ordinary fluid. The velocity variation of the granular particles is expressed by $\langle v(h) \rangle = v_0 \exp(-h/h_0)$ as a function of depth h from the pile's surface, where v_0 and h_0 are constants and $\langle \cdot \rangle$ is temporal average. Similarly to Eqs. (6) and (7), the exponential time scale variation is formed from the surface to the inside of the sandpile.

Since our model mainly concerns with the reaction, we discuss such time scales variation, in the reaction-diffusion systems. This is possible when the concentration of some chemical that plays the role of time scale factor such as catalytic activity in the system, changes gradually in space in this reaction-diffusion process. For example, we assume a chemical C catalyzes all the reaction process in the system, including the diffusion process of other molecules. For simplicity, we assume that the reaction in Eq. (3), the flow $\partial b/\partial x$ and the diffusion $\partial^2 b/\partial x^2$ in Eq. (5) are in the previous section are catalyzed by the chemical C. Besides this catalytic process, the chemical by itself is degraded as



and diffuses in space. From one end of the boundary in the one-dimensional space, chemical C is supplied. Then Eq. (5) and the these characteristics are integrated as

$$\begin{cases} \frac{\partial a}{\partial t} = (k_1 - ab^2)c \\ \frac{\partial b}{\partial t} = (ab^2 - k_2b)c + cv_g \frac{\partial b}{\partial x} + cD_b \frac{\partial^2 b}{\partial x^2} \\ \frac{\partial c}{\partial t} = -k_c c + D_c \frac{\partial^2 c}{\partial x^2} \end{cases} \quad (11)$$

where c is the concentration of C. As the boundary condition of C, $c = \text{const.} > 0$ at $x = 0$ and $c = 0$ in $x \rightarrow \infty$ are adopted. The reaction diffusion equation for c is calculated.⁵ Then, exponential concentration gradient is derived as

$$c(x) = \text{const.} \times \exp\left(-\sqrt{\frac{k_c}{D_c}}x\right) \quad (12)$$

Here the degradation Eq. (10) plays as a similar role to the void creation in the velocity time scale variation in the sand pile. The boundary condition at $x = 0$ is adopted as $\text{const.} = 1$, and Eq. (11) is transformed as

$$\begin{cases} \exp\left(\sqrt{\frac{k_c}{D_c}}x\right) \frac{\partial a}{\partial t} = k_1 - ab^2 \\ \exp\left(\sqrt{\frac{k_c}{D_c}}x\right) \frac{\partial b}{\partial t} = ab^2 - k_2b + v_g \frac{\partial b}{\partial x} + D_b \frac{\partial^2 b}{\partial x^2} \end{cases} \quad (13)$$

The equations correspond to Eq. (6) with $\sqrt{k_c/D_c} = k_x$.

Another route for the introduction of the time scale variation is the gradient of temperature. Often the reaction rate has exponential dependence on the temperature T . Indeed, if the dependence is of the form $\exp(-\text{const.}/T(x))$ with $T(x) = T_0 + \delta T(x)$ for small δT , the rate change as $\exp(-\text{const.} \times \delta T(x)/T_0^2)$. Then, if the temperature has a gradient from one side to another, the exponential dependence of the parameters on the space as in the model is derived.

3.3. Dynamics without time scale variation

As a basis for further studies of a system with time scale variation introduced in Eq. (8), we first survey the convective instability in the system without time scale variation. That is, $T_i = 1$ in Eq. (7) as

$$\begin{cases} \dot{a}_i = k_1 - a_i b_i^2 \\ \dot{b}_i = a_i b_i^2 - k_2 b_i + v(b_{i-1} - b_i) \end{cases} \quad (14)$$

is briefly reported. Without noise, there is neither a stable limit cycle nor any other fixed point beside the above fixed point, for any initial conditions. When Gaussian white noise η which satisfies

$$\langle \eta(t)\eta(t - \tau) \rangle_t = \delta(\tau)\sigma^2 \quad (15)$$

is applied at the upstream, noise is spatially amplified and transmitted from the upstream to the downstream, and the NSS with a large amplitude is generated at the downstream, as shown in Fig. 1(a), which Fig. 1(b) displays spatial development of the fluctuation measured by the root mean square (RMS) of b_i as

$$V(i) \equiv \sqrt{\langle b_i^2 \rangle - \langle b_i \rangle^2} \quad (16)$$

where $\langle \cdot \rangle$ denotes the temporal average. $V(i)$ gives a measure of the degree of temporal variation of the element, or, in other words, the amplitude of the oscillation. $V(i)$ exponentially increases with i before it saturated, and the spatial amplification rate is calculated by

$$\Lambda^S(i) \equiv \log \frac{V(i)}{V(i-1)} \quad (17)$$

Spatial instability exponent λ^S calculated from Eq. (2) (by $\lambda^S = 0.32$) shows good agreement with the rate of amplification Λ^S for small perturbation along the space, obtained numerically, i.e.,

$$\lambda^S \simeq \Lambda^S \quad (18)$$

⁵ Without the degradation term $-k_c c$, linear concentration gradient is derived.

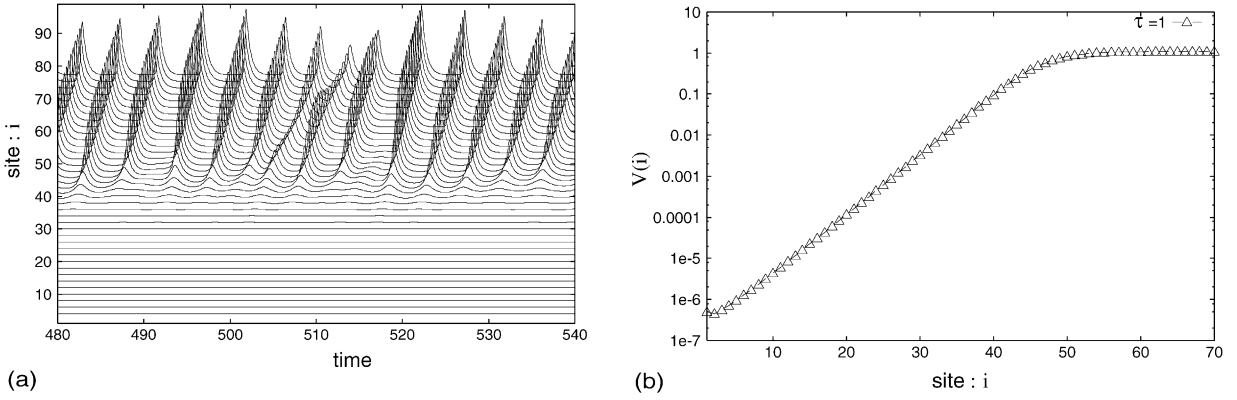


Fig. 1. (a) Spatiotemporal plot of $b_i(t)$ without time scale variation under application of Gaussian noise η at $i = 1$. NSS is generated at $i \sim 40$. (b) Corresponding RMS of $b(i)$, $V(i)$, is plotted as a function of i . $|\eta| = 10^{-6}$, $k_1 = 1.01$, $k_2 = 1.5$ and $v = 4$.

The site $i = i_g$ defined as the site where the NSS is generated is given by [20,22]

$$\sigma \exp \left(\sum_i^{i_g} \lambda^S \right) \simeq \sigma \exp \left(\sum_i^{i_g} \Lambda^S \right) = \sigma \frac{V(i)}{V(0)} \sim 1 \quad (19)$$

because of $V(0) \sim \sigma$ and $V(i_g) \sim O(1)$. This estimate agrees well with that obtained numerically.

When a periodic input is applied from one end in such system, the amplification rate of such input depends on the frequency in general. This amplification rate is computed as that of the Fourier component ψ_i , the component of Fourier transform of linearized each variable. The degree of the convective instability to periodic perturbation with frequency f , i.e., $\kappa(f)$, is defined as the amplification rate of the component per space i . This rate is computed in Appendix A. By inserting Eq. (14) into Eq. (A.1), Eq. (A.5) is calculated as

$$\begin{cases} (2\pi j f + b_*^2) \psi_{i,a} + 2a_* b_* \psi_{i,b} = 0 \\ -b_*^2 \psi_{i,a} + (2\pi j f - 2a_* b_* + k_2 + v) \psi_{i,b} = v \psi_{i-1,b} \end{cases} \quad (20)$$

where (a_*, b_*) satisfied with $\dot{A}_i = 0$, $(a_*, b_*) = (k_2^2/k_1, k_1/k_2)$. From Eq. (20), the term $\psi_{i,a}$ is eliminated, to get the recursive equation. The degree of convective instability to periodic perturbation with frequency f is then given by

$$\kappa_i(f) \equiv \log \left| \frac{\psi_{i,b}(f)}{\psi_{i-1,b}(f)} \right| = \frac{1}{2} \log \frac{v^2 ((2\pi f)^2 + (k_1/k_2)^4)}{((2\pi f)^2 - (k_1/k_2)^2(k_2 + v))^2 + (2\pi f)^2((k_1/k_2)^2 - k_2 + v)^2} \quad (21)$$

Fig. 2 shows $\kappa(f)$ calculated from Eq. (21) for $v = 4$. As shown, $\kappa(f)$ takes a positive value in some range of f , e.g., $f_{\min} < f < f_{\max}$, but is negative for $0 \leq f < f_{\min}$ and $f_{\max} < f < \infty$.⁶ In other words, each element works as a band pass filter [32] in the frequency range so that the fluctuation only with the frequency $f_{\min} < f < f_{\max}$ is amplified and transmitted to the downflow. This property of $\kappa(f)$ is necessary for the time scale translation of the fluctuation as will be reported in the present paper.

⁶ This result is in a good agreement with the numerical estimate, measured as the spatial amplification rate $\log V(i)/V(i-1)$ when $A \sin(2\pi f t)$ ($A \ll 1$) is applied at the boundary condition, instead of the Gaussian noise.

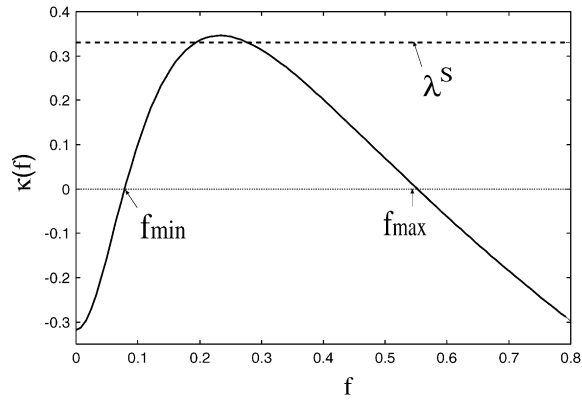


Fig. 2. The degree of the convective instability to periodic perturbation with frequency f , defined by $\kappa(f)$, is plotted as a function of f . f_{\max} and f_{\min} are defined as the frequency satisfied with $\kappa(f) = 0$. The dotted line denotes $\lambda^S = 0.32$.

4. Convective instability with time scale translation

In the section, convective instability and NSS in an open flow system with time scale variation, i.e., Eq. (7), are presented.

In this system, without noise, all elements converge to the unique fixed point $(a_i, b_i) = (a_*, b_*)$, as in the model without time scale variation, Eq. (14). Even under the time scale difference, the convective instability is still

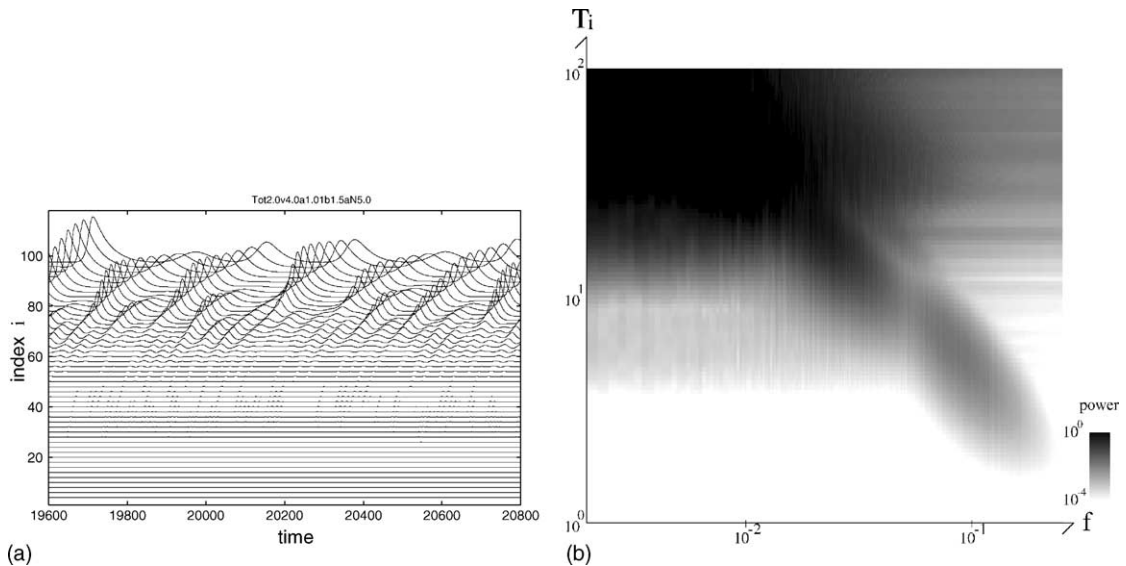


Fig. 3. (a) Spatiotemporal plot of $b_i(t)$ and (b) the power spectrum by gray scale. (a) Time series of elements are plotted, by putting them in the order of the index i from the lower column to higher, i.e., lower column shows b_i of faster elements. (b) Abscissa axis denotes the frequency f , and the ordinate axis denotes the characteristic time scale T_i of each element, while the gray scale shows the power spectrum of the corresponding frequency and the corresponding element i . From the upstream (the lower side) to the downstream (the upper side), the shift of the peak frequency of each element shift is detected from high to low frequency. The peak values increase as shown in the increase of darkness, showing the spatial amplification of the fluctuation by the convective instability. $(L, \tau) = (100, 1.05)$, $|\eta| = \sigma = 10^{-5}$. The value of v, k_1 and k_2 are same as those for Fig. 1.

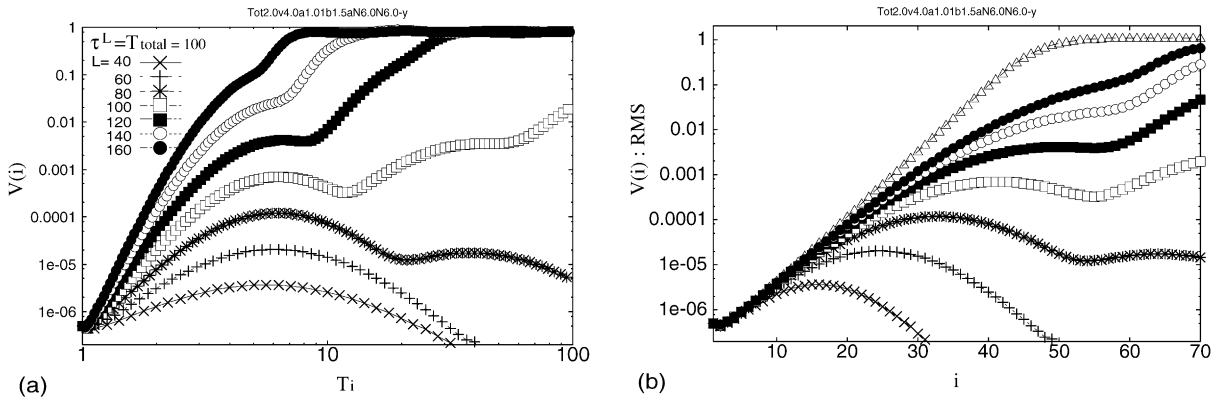


Fig. 4. The spatial development of $V(i)$ is plotted as a function of T_i in (a) and i in (b), where small Gaussian noise η with the amplitude $\sigma = 10^{-6}$ is applied at $i = 0$. The marks correspond to different values of (L, τ) as shown in the legend, while in (b) the data for $\tau = 1$ are also plotted as Δ , for reference. For larger τ , the amplification rate of $V(i)$ by element or by time scale decays towards 0. Accordingly, the NSS, which appears at $V(i) \sim 1$, is difficult to be generated at the downstream. The value of v, k_1 and k_2 are same as those for Fig. 1.

maintained. Hence, when small Gaussian noise η (with the amplitude $\sigma \ll 1$) is applied at $i = 1$, the NSS is generated at the downstream, as shown in Fig. 3 for $(L, \tau) = (100, 1.05)$. In the figure, the values of v, k_1 and k_2 are same as those adopted in Fig. 1, and the degree of exponential time scale gradient is $k_x = \log \tau = 2.0 \times 10^{-2}$, where spatiotemporal plot of $b_i(t)$ is given in Fig. 3(a) and the corresponding power spectra for all elements are given in Fig. 3(b) by using the gray scale. In (b), abscissa axis denotes frequency and ordinate axis the characteristic time scale of each element T_i . As shown, the peak of the spectra is sharper as the peak frequency is shifted to smaller frequency, as the element goes to downstream. With this shift, the peak amplitude also increases, as is seen in the increase of the darkness in the figure. Note that the peak at a lower frequency at downstream is produced, even if we apply a high-pass filtered noise, instead of white noise, at the upstream element, so that the low frequency component does not exist at all, at an upper stream element.

The result shows that the upstream disturbance is not only spatially amplified but is also transmitted, successively translated into a slower time scale, i.e., the convective instability allows for the time scale translation of the transmitted fluctuation.

Fig. 4 shows the spatial development of the RMS $V(i)$. Recall that for $\tau = 1$, $V(i)$ increases exponentially (as is characterized by the spatial instability exponent λ^S) as already shown in Fig. 1. As τ is increased, the spatial amplification rate of $V(i)$, namely, $\Lambda^S(i)$, decreases. Accordingly a clear NSS is hardly generated. Instead, $V(i)$ shows an oscillatory change, as shown in Fig. 4(b). Note also that the NSS is no longer generated if τ is too large. Only for a range of values of $\tau (>1)$, the transmission of fluctuation with the time scale translation is possible.

5. Mechanisms for the convective instability

In this section, we analyze the process how the time scale of the fluctuation is made slower through the spatial transmission to the downstream.

Since inherent time scale of the downflow dynamics is slower, the upstream fluctuation effectively has a higher frequency viewed from the time scale of the downflow. For some motion to be propagated to the downflow, it is then necessary that the time scale of fluctuation as well as some oscillatory motion should be translated into a slower time scale. In the present section, we first show that the fluctuation cannot keep on being amplified, unless such translation to longer time scale appears. Then, we will show that a bifurcation leading to time-scale multiplication provides a mechanism of such translation here, in a similar way to period-doubling bifurcation. With this mechanism, some

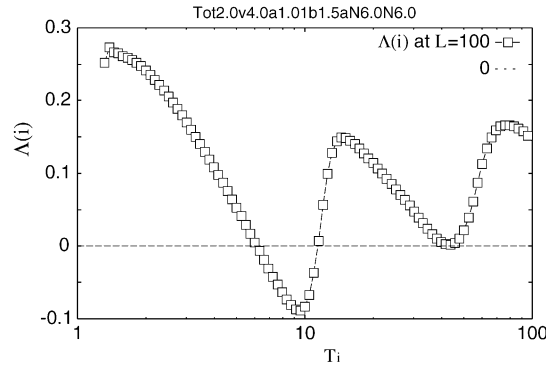


Fig. 5. Spatial development of $\Lambda^S(i) = \log(V(i)/V(i-1))$ as a function of T_i is plotted under the application of Gaussian noise at $i = 1$. k_1, k_2, v, σ and $(L, \tau) = (100, 1.05)$ are same as those for \square in Fig. 4(a). It shows damped oscillation around $\Lambda^S(i) = 0$ and smaller than $\lambda^S = 0.32$ with $\tau = 1$.

property in the fast dynamics is translated to the dynamics of slower time scale. Accordingly, the slow dynamics can show sensitive dependence on the fast fluctuation in the upstream fast dynamics, as will be discussed in Section 6.

To study the present issue, we first need to characterize the position (i.e., the time scale) dependence of the spatial amplification rate of fluctuation. For it, we study the relation between λ^S and Λ^S in the system with the time scale variation. As described in Section 3.1, Λ^S shows good agreement with λ^S for $\tau = 1$. Fig. 5 shows $\Lambda^S(i)$ as a function of T_i where $V(i) < 10^{-2} \ll 1$ with $(L, \tau) = (100, 1.05)$ corresponding to \square in Fig. 4. $\Lambda^S(i)$ decreases from the value $\lambda^S (= 0.32)$, as the site i goes down flow. This is expected, since $\kappa(f)$ decreases for larger f , and the fluctuation at the upstream is in a high frequency regime for the downflow element. For the further down flow site, however, $\Lambda^S(i)$ increases again, until it decreases again. The oscillation of $\Lambda^S(i)$ around 0 is observed when $\tau > 1$.

In the following subsections, we will show the mechanism of the oscillation of $\Lambda^S(i)$. First, this oscillation will be shown to be induced by bifurcation that produces a motion of a longer period. With this bifurcation, time scale is translated to a slower motion. This bifurcation with the time scale multiplication of the fluctuation is repeated. A single cycle of the oscillation $\Lambda^S(i)$ corresponds to each bifurcation.

The organization of later subsections is as follows. In Section 5.1, we analyze the dependence of the convective instability on the time scale of the fluctuation by measuring $\Lambda^S(i)$ and $\kappa(f)$. In Section 5.2, we report the time scale multiplication of the transmitted fluctuation that appears when $\Lambda^S(i)$ changes from positive to negative. By the time scale multiplication, the characteristic time scale of the fluctuation gets slower. In Section 5.3, the length of the multiplication cycle is analyzed in relation to $\kappa(f)$ as shown in Fig. 2. In Section 5.4, through these analysis, we derive the conditions for the NSS with the time scale multiplication of the transmitted fluctuation in the open flow system with the time scale variation.

5.1. Measure of the convective instability

In this subsection, we introduce the measure of the convective instability in a system with time scale variation. First, we extend the result on the degree of the convective instability to periodic perturbation $\kappa(f)$ in Section 3.1 to the case with $\tau > 1$. Second, under the application of the Gaussian noise at the upstream, $\Lambda^S(i)$, the degree of the convective instability, is shown to agree well with $\kappa(f = (\bar{\Delta}(i)/T_i)^{-1})$, where $\bar{\Delta}(i)$ is the temporal average of the time scale of the fluctuation introduced later.

We numerically check the spatial amplification rate of the oscillation amplitude under the periodic perturbation $A \sin(2\pi t/T_0)$ ($A \ll 1$), which corresponds to $\kappa(f)$ in the case with $\tau = 1$ given in Fig. 2. Here, because the noise is not applied, the periodicity is maintained as a transmission of wave with the period T_0 . The amplification rate is

in good agreement with the analytic results, i.e., $\kappa(f = (T_i/T_0)^{-1})$, where $(T_i/T_0)^{-1}$ denotes the inverse of the time scale of the perturbation period normalized by the intrinsic time scale of each element T_i .

Here we study the relation between $\kappa(f)$ and $\Lambda^S(i)$ under the application of Gaussian noise η applied at $i = 1$. First, as a measure of the inherent time scale of the fluctuation at each element, we introduce the average time scale of the fluctuation of $b_i(t)$ as $\bar{\Delta}(i)$. The method for the computation is described in Appendix B. Then, the normalized average frequency \bar{f}_i is expressed as

$$\bar{f}_i = \left(\frac{\bar{\Delta}(i)}{T_i} \right)^{-1} \quad (22)$$

It corresponds to the peak frequency at each element in Fig. 3(b).

Second, $\Lambda^S(i)$ is measured by the convective instability of the fluctuation around (a_*, b_*) . To compare this quantity with $\kappa(\bar{f}_i)$, we define the frequency corresponding to each site i , which is given by \bar{f}_i defined above. Then the rate of amplification for each site i is estimated by the rate of amplification of the frequency given by $\kappa(f)$. Indeed,

$$\Lambda^S(i) \simeq \kappa(\bar{f}_i) \quad (23)$$

holds rather well up to some sites. In Fig. 6, $\Lambda^S(i)$ and $\kappa(\bar{f}_i)$ are shown as a function of T_i . This degree of spatial amplification of fluctuation, $\Lambda^S(i)$, agrees rather well with $\kappa(f)$. In other words, the decrease of the spatial instability along the site is well characterized by the change of effective frequency of fluctuation, due to the change of the time scale of each element.

As shown in Fig. 5, this decrease stops at some site. Indeed, there, the effective frequency of fluctuation starts to decrease as is also shown in Fig. 6. Here the time scale multiplication of the fluctuation occurs as will be discussed in detail at the next subsection. By the multiplication, \bar{f}_i is decreased, and the corresponding $\kappa(\bar{f}_i)$ is increased. Accordingly $\Lambda^S(i)$ becomes positive again, and the convective instability is restored. Once the convective instability sufficiently is restored, the fluctuation is amplified and transmitted without the multiplication. This amplification rate is again estimated well by $\kappa(\bar{f}_i)$, which decreases again with the increase of \bar{f}_i along the downflow, in Fig. 6. This cycle of decrease of $\Lambda^S(i)$ and recovery to a positive value by period multiplication is repeated.

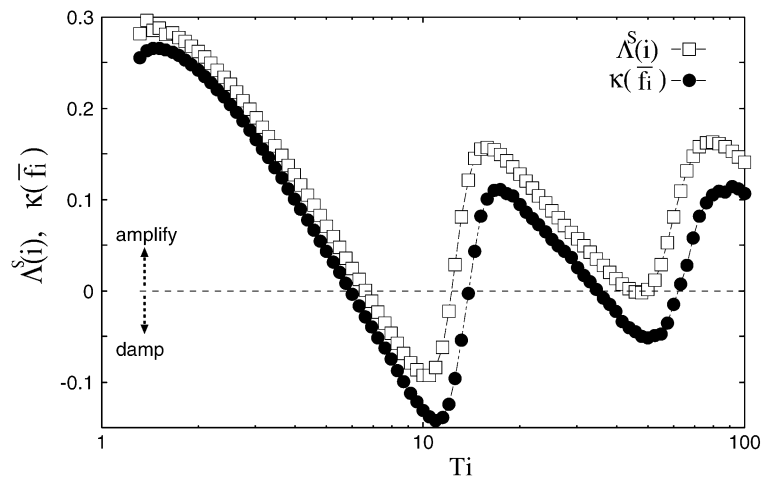


Fig. 6. $\Lambda^S(i)$ and $\kappa(\bar{f}_i)$ are plotted as a function of T_i . They are rather good agreement with each other. The values of $k_1, k_2, v, (L, \tau)$ and σ are same as those for Fig. 5.

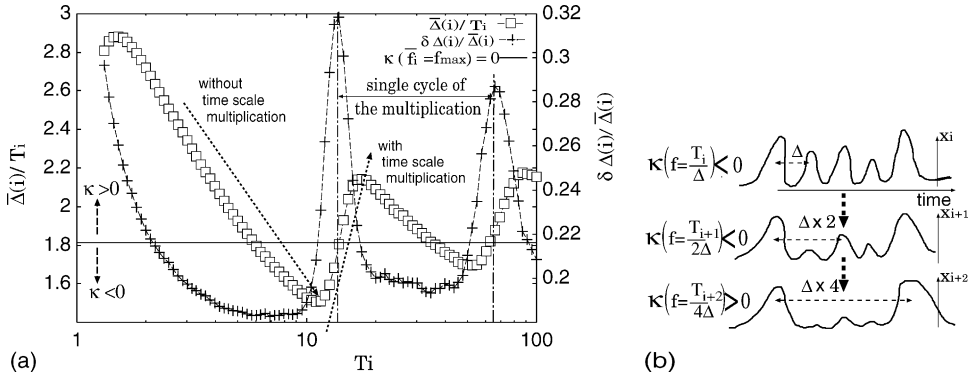


Fig. 7. (a) $\bar{\Delta}(i)/T_i$ (\square) and $\delta\Delta(i)/\bar{\Delta}(i)$ ($+$) as a function of i . The value of $k_1, k_2, v, \tau, L, \sigma$ are same as those for Fig. 5. (b) The schematic representation of the time scale multiplication process.

5.2. Time scale multiplication of the transmitted fluctuation

In this subsection, we show that the origin of the oscillation of $V(i)$ in Fig. 5 is the time scale multiplication of the transmitted fluctuation. As schematically shown in Fig. 3(b), the time scale multiplication is a bifurcation to eliminate a motion with a higher frequency of motion. This multiplication is observed as the site goes downflow. We study the process through the analysis of the average time scale $\bar{\Delta}(i) \equiv \langle \Delta_s(i) \rangle_s$ and the RMS $\delta\Delta(i) \equiv \sqrt{\langle \Delta_s(i)^2 \rangle_s - \langle \Delta_s(i) \rangle_s^2}$ of $b_i(t)$. See Appendix B for the specific method for the computation of these quantities.

Fig. 7(a) shows $\bar{\Delta}(i)/T_i$ and $\delta\Delta(i)/\bar{\Delta}(i)$ as a function of T_i . Around $T_i \sim 12$ and 60 , $\bar{\Delta}(i)/T_i$ takes local minima, and then for larger T_i , it shows a steep increase, and at slightly larger values of T_i , $\delta\Delta(i)/\bar{\Delta}(i)$ takes local maxima. This rapid increase of $\bar{\Delta}(i)/T_i$ corresponds to the time scale multiplication. The time scale multiplication process is also shown in Fig. 3(a), where some pulses disappear at some element. Accordingly, the time scale of the transmitted dynamics is made slower. This multiplication of time scale appears repeatedly from the upstream to the downstream, as also shown in Fig. 6.

Fig. 7(b) shows the schematic representation of the time scale multiplication process described above. As it goes to the downstream, T_i increases and the normalized time scale of the fluctuation $\bar{\Delta}(i)/T_i$ decreases, as shown, for example, for $T_i \lesssim 10$ in Figs. 6 and 7(a). Accordingly, $\kappa(\bar{f}_i)$ changes from positive to negative value at some element with $T_i \sim 6$.

For an element with $\kappa(\bar{f}_i) < 0$, the distribution of $\Delta(i)$ gets broader, i.e., $\delta\Delta(i)/\bar{\Delta}(i)$ gets larger as shown in Fig. 7(a). Within the broad distribution of $\Delta(i)$, some pulses are spatially damped and disappear, since $\kappa(\bar{f}_i) < 0$. This occurs for $\Delta/T_i < f_{\max}^{-1} = 1.8$, where Δ denotes the time interval of each pulse in the fluctuation as shown in Fig. 7(b). Accordingly the time scale of survived pulses gets slower. Then, for the transmitted wave, the convective instability is regained, the condition for the instability is satisfied for the normalized time scale, $\Delta/T_i > f_{\max}^{-1} = 1.8$ again.

Here we define the multiplication ratio as the ratio of T_i 's for successive local minima. In this example, the multiplication ratio per a single cycle is $60/12 \sim 5$ here, as shown in Fig. 7(b). This roughly gives the rate of frequency reduction by each multiplication process (recall also Fig. 6). By the repetition of the time scale multiplication, the fluctuation of fast elements can be translated into slower time scale, and transmitted to the downstream slow elements.

The noise η is essential for the time scale multiplication process. When only periodic perturbation $A \sin 2\pi t/T_0$ is applied at the upstream, periodicity is just maintained and transmitted. Accordingly, at some site i_* , normalized time scale of the dynamics $\bar{f}_{i_*} = T_0/T_{i_*}$ becomes smaller than f_{\max}^{-1} , satisfying $\kappa(\bar{f}_i) < 0$. Then variance of the element $V(i) = \sigma \exp(\sum_i \Lambda^S(i)) \simeq \sigma \exp(\sum_i \kappa(\bar{f}_i))$ (cf., Eqs. (17) and (23)) decreases towards 0, as i is larger. On the other hand, aperiodicity of the transmitted fluctuation leads to the broader distribution as shown in Fig. 7(a), and

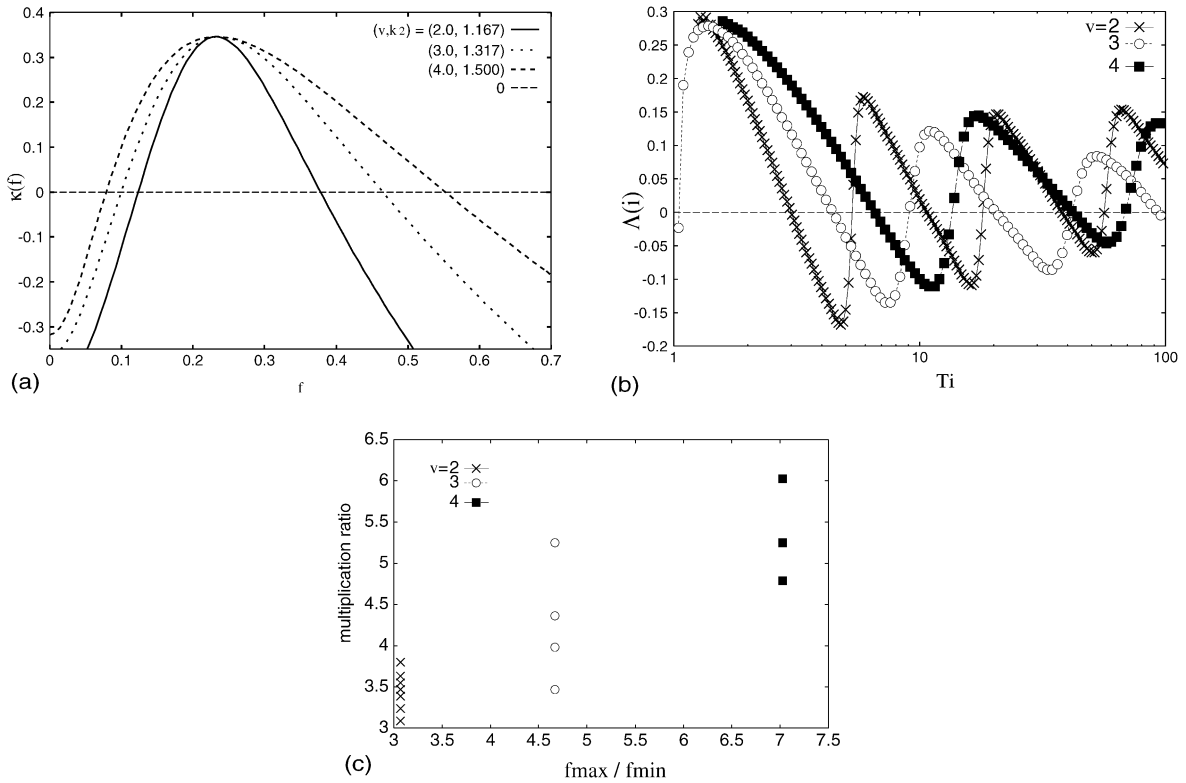


Fig. 8. (a) $\kappa(f)$ for a different set of values $(v, k_2) = (2, 1.167)$ (bold line), $(3, 1.317)$ (dotted line), $(4, 1.5)$ (broken line). Although k_2 is set so that $\max_f \kappa(f)$ is independent of v , f_{\max} , f_{\min} and the ratio f_{\max}/f_{\min} depend on v . (b) $\Lambda(i)$ under the application of Gaussian white noise at $i = 1$ as a function of T_i for $v = 2, 3, 4$. Each mark corresponds to each line in (a) as shown in the legend of the both figures. The period of oscillation, i.e., the rate of the frequencies by multiplication changes with v . (c) The multiplication ratio, plotted as a function of f_{\max}/f_{\min} . It is measured by ratio among the time scales where $\delta\Delta(i)/\bar{\Delta}(i)$ shows local maxima as shown in Fig. 7(b), for various strength of the noise. The marks are same as (b). (L, τ) and k_1 are same with the marks.

allows for disappearance of some pulses through the transmission of the wave. Then, the time scale multiplication is possible to make the time scale longer.

5.3. Cycle of the multiplication

Here we study the relationship of multiplication ratio with $\kappa(f)$. Fig. 8(a) shows $\kappa(f)$ as a function of f , as in Fig. 2, for various v . f_{\max} , f_{\min} and the ratio f_{\max}/f_{\min} depend on v . Correspondingly we have computed the model Eq. (7) by applying Gaussian white noise at $i = 1$, to obtain spatial development of $\Lambda(i)$, as is plotted as a function of T_i in Fig. 8(b). The period of oscillation along the space, i.e., the multiplication ratio, changes with v .

As already mentioned, this multiplication ratio is highly correlated with the reduction of the frequency of the transmitted fluctuation by the multiplication. Recalling Fig. 6, we can say that the multiplication process occurs when the corresponding $\kappa(\bar{f}_i)$ becomes negative, while by the multiplication, the corresponding $\kappa(\bar{f}_i)$ again takes a large positive value. Then, it is expected that the multiplication ratio is correlated with f_{\max}/f_{\min} for $\kappa(f)$. In Fig. 8(c), the multiplication ratio is plotted as a function of f_{\max}/f_{\min} . As expected, the ratio increases monotonically with f_{\max}/f_{\min} .

As f_{\max}/f_{\min} gets larger, the multiplication ratio, i.e., the period for successive multiplication events increases. The event of multiplication is less frequent. Accordingly, the multiplication influences less on the fluctuation in the downstream.

Furthermore, when f_{\min} does not exist, i.e., if $\kappa(0) > 0$, any lower frequency fluctuation than f_{\max} is amplified and transmitted without the time scale multiplication, though the time scale multiplication can still appear for higher frequency. The time scale translation to slower scale by the multiplication is then blurred by the amplification without the multiplication. Accordingly regular structure is no longer produced at the downflow.

To sum up, existence of $f_{\min} > 0$ and not too large ratio f_{\max}/f_{\min} is necessary for successive appearance of the multiplication, to produce NSS at the downflow. Meaning of this condition will be discussed again at Section 6.4.

5.4. Conditions for the noise-sustained structure with time scale multiplication

In the previous three subsections, we have shown that the time scale multiplication leads to the propagation of the noise sustained structure, to a slower time scale. Summarizing the result of the above three subsections, we state the conditions for it.

As described in Section 5.1, the convective instability with time scale variation is well characterized by $\kappa(\bar{f}_i)$. Adopting $\kappa(\bar{f}_i)$ instead of λ^S from Eq. (23), we extend Eq. (19) for the open flow with time scale variation as Eq. (7) given by

$$\sigma \exp\left(\sum_{i=1}^{i_g} \kappa(\bar{f}_i)\right) \sim 1 \quad (24)$$

In our model Eq. (7), the condition for the NSS through the time scale multiplication, namely, Eq. (24), is satisfied under the following three properties.

- As shown in Fig. 2, the degree of convective instability depends on the frequency of the transmitted fluctuation with the frequency f as

$$\max_f \kappa(f) > 0, \quad \lim_{f \rightarrow \infty} \kappa(f) < 0 \quad (25)$$

The former is necessary for the convective instability and the latter for damping of faster fluctuation than the scale T_i (i.e., $\kappa(f) < 0$ for $f = (\Delta/T_i)^{-1} > f_{\max}$ as shown in Fig. 2). In the present model, these conditions hold for a given range of the parameters, v , k_1 and k_2 .

The latter condition is not satisfied, for example, in a unidirectionally coupled complex Ginzburg–Landau oscillator model, instead of Eq. (4). For the model within some range of parameters, the condition $\max_f \kappa(f) > 0$ is satisfied, but $\lim_{f \rightarrow \infty} \kappa(f) = 0$. In this case, for a system with time scale variation such as Eq. (7), the time scale multiplication of the transmitted fluctuation cannot appear.

- The existence of $f_{\min} > 0$, namely,

$$\kappa(0) < 0 \quad (26)$$

and the ratio f_{\max}/f_{\min} is not too large as discussed in Section 5.3. These conditions are necessary for the appearance of the multiplication effect in the downstream fluctuation.

- The motion of the transmitted fluctuation is not periodic, described in Section 5.2. This is necessary to have broad power spectrum so that faster motions are only eliminated, leading to a bifurcation with a slower time scale dynamics. This condition is necessary for the time-scale multiplication.

6. Sensitive dependence of slow dynamics on fast elements

In this section, we report how fast elements in the upstream affect the slow dynamics in the downstream, by the time scale multiplication of the transmitted fluctuation, as described in the above sections.

6.1. Numerical results

First we will show how statistical property of the slowest dynamics depends on that of fastest one by making the following operation to the fastest element, as introduced in the references [10]. In order to check the influence of the change of the fastest element, we apply some input to the upstream, and see how it affects the dynamics of the downstream. We set up the following external operation, and study the response.

6.1.1. External operation and response

After the initial transients have died out, at an arbitrarily chosen point in the temporal evolution, we apply periodic input $A \sin(2\pi t/T_0)$ ($A \ll 1$, $T_0 \sim T_1$) and Gaussian noise η (with the strength $\sigma \ll 1$) at the most upstream element, $i = 1$, where the time scale T_0 is the order of that of the upstream ($T_0 \sim T_i$). Then we examine if this addition of an external input to the upstream influences the downstream with a slower time scale.

Fig. 9 shows the spatiotemporal plot when T_0 is changed from 6 to 12 at time = 20,000. At the downstream, NSS is generated following this change of T_0 , through the repeated time scale multiplication of the transmitted pulses. Recall again that the time scale of the downstream dynamics is of the order of 10^2 , that is much slower than T_0 .

The plot in Fig. 9 shows that the time scale of the NSS generated at the downstream is of the order of the time scale of each element, and is much larger than the input time scale T_0 , as in Fig. 3(a). To study the amplitude of generated oscillation, we again adopt $V(L)$, the RMS of b_L of the slowest element. Fig. 10(a) shows the spatial development of $V(i)$ by changing the frequency of the periodic inputs and noise applied

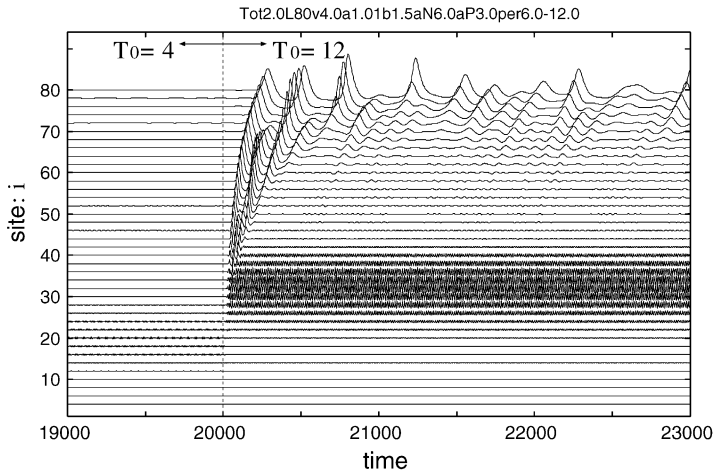


Fig. 9. Spatiotemporal plot of b_i , when T_0 is changed from $T_0 = 6$ to $T_0 = 12$ at time = 20,000, where T_0 is the input period applied at $i = 1$ given by $A \sin(2\pi t/T_0)$ with Gaussian noise η . The plotting methods and the axes are identical with Fig. 3(a). The NSS that does not exist for $T_0 = 6$, is generated at the downstream with the change to $T_0 = 12$. $|\eta| \equiv 10^{-6}$, $A = 10^{-3}$, $T_{\text{total}} = 100$, $(L, \tau) = (80, 1.06)$. The value of v , k_1 and k_2 are same as those for Fig. 1.

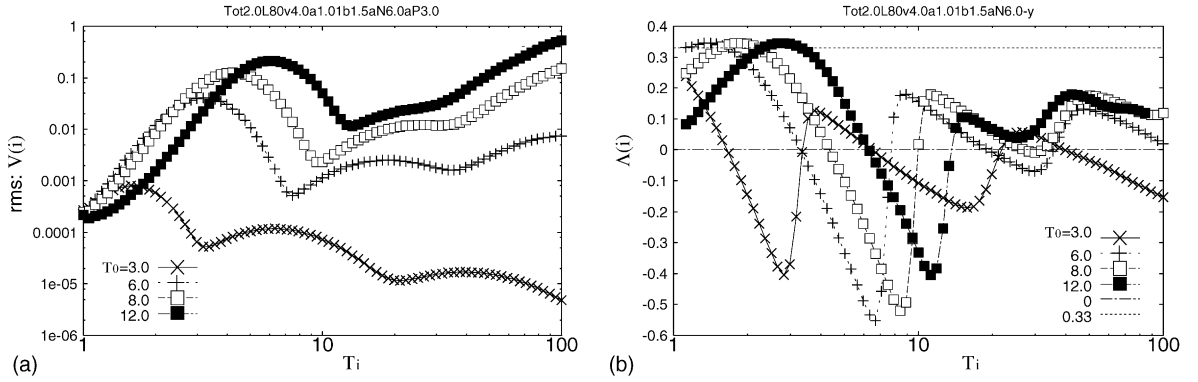


Fig. 10. RMS of $b_i(t)$ in (a) and the corresponding $\Lambda^S(i)$ in (b) are plotted as a function of T_i , where Gaussian noise η and $A \sin(2\pi t/T_0)$ is applied at $i = 1$. Each symbol in the plot corresponds to a different value of T_0 as shown in the legend. (a) They show oscillation corresponding to the time scale multiplication of the transmitted fluctuation. (b) The phase of the oscillation and average of $\Lambda^S(i)$ is plotted for the same set of input periods T_0 , using the same symbol. The same values of (L, τ, A) and σ are chosen as those for Fig. 9.

at $i = 1$.⁷ The difference of $V(i)$ by the input period at $i = 1$ is amplified (exponentially) in space. Then a larger difference is generated at the downstream. In other words, the amplitude of the element of the slow scale measured by $V(L)$ sensitively depends on the period of the input at the fastest element.

As shown in Fig. 10(b) the pattern of $\Lambda^S(i) = \log V(i)/V(i-1)$ depends on the period T_0 of the upstream. There, as T_0 is larger, the amplitude of the oscillation of $\Lambda^S(i)$ is larger. The oscillation is maintained even at the downstream. The summation $\sum_1^i \Lambda^S(i)$ at the downstream changes accordingly. Since the amplitude of the oscillation $V(i)$ is expected to increase as $\sigma \exp(\sum_1^i \Lambda^S(i))$, it is sensitively dependent on T_0 , as shown in Fig. 10(a). Hence, the downstream slow dynamics shows *sensitive* dependence on the upstream fast dynamics characterized by T_0 .

6.2. The boundary condition sensitivity in an open flow system

In this subsection, we briefly review the condition for the boundary condition sensitivity [28,29], discussed generally for an open flow system.

In general, we consider a unidirectionally coupled oscillator system given by $d\vec{A}_i/dt = \vec{F}(\vec{A}_i, \vec{A}_{i-1})$, where $\vec{A}_i = (a_i, b_i)$ and system size is L . Assume that each element, without adding noise, is attracted to a unique fixed point for any initial conditions. Generally, the value of this fixed point depends on the site i . When viewed from upstream to downstream, this spatial sequence of the fixed points is represented by a relaxation process from a fixed boundary condition \vec{A}_0 to a fixed point \vec{A}_* , at the downstream, that is independent of \vec{A}_0 . On the other hand, by the application of Gaussian noise η ($|\eta| \ll 1$), the property of the downstream dynamics, for example, the amplitude or frequency of the NSS, characterized by the RMS $V(L)$ of \vec{A}_L , can depend on the value of the boundary condition. This phenomenon is called noise-induced boundary condition dependence. This boundary dependence is maintained even if a small noise is applied at all the elements. In other words, this sensitive dependence is both noise-induced and tolerant to noise.

According to the spatial relaxation pattern of the fixed points, the degree of the convective instability of the fixed points, quantitatively characterized by $\lambda^S(i)$ in Eq. (2) of the upstream depends on the boundary condition \vec{A}_0 . On the other hand, the degree of convective instability is independent of the boundary where the fixed point approaches

⁷ In the upstream, $V(i)$ mainly shows the amplitude with period T_0 rather than noise η , because of $A > \sigma$. In $T_i \lesssim 2$, $V(i)$ is spatially amplified because of the convective instability satisfied with $T_0/T_i > 1/f_{\max}$ as described in Section 5.2. On the other hand, in $T_i \gtrsim 2$, $V(i)$ is spatially damped because of the absolute stability satisfied with $T_0/T_i < 1/f_{\max}$.

Table 1

Correspondence of the boundary condition dependence in the open flow without time scale variation to initial condition dependence in a $1 - d$ chaotic map $x_{n+1} = f(x_n)$

Each step	Space (i)	Time step (n)
Initial state	Upstream property \bar{A}_0, σ	x_1
Final state	Downstream property RMS of \bar{A}_L	x_N
Instability	Convective instability $\lambda^S(i)$	Temporal instability $\log dx_{n+1}/dx_n $
Difference on initial state	Value of the boundary $\delta\bar{A}_0$	Value δx_1
Initial state sensitivity	$\sum_{i=1}^{i=i_g} \{ \lambda^S(i) _{\bar{A}_0+\delta\bar{A}_0} - \lambda^S(i) _{\bar{A}_0} \}$	$\delta x_1 \exp(\sum_{n=1}^{n=N} \log dx_{n+1}/dx_n)$
Condition	$i_g \lesssim i_r$	$\delta x_1 \exp(\sum_{n=1}^{n=N} \log dx_{n+1}/dx_n) > 1$

\bar{A}_* in the downstream. If $\lambda^S(i)$ relaxes spatially to the value for the downstream fixed point before NSS is generated, then there is no boundary condition dependence. Hence, only if the scale i_g , defined in Eq. (19) as the formation length for the NSS, is smaller than the scale for the above length for the spatial relaxation, the generated downstream dynamics is expected to depend on \bar{A}_0 .

As a simple measure of the spatial relaxation length i_r of the fixed points, we have introduced a ‘half-decay’ length for the spatial relaxation of $\lambda^S(i)$ [28]. Roughly speaking, $\lambda^S(i)$ is sensitively dependent on the boundary \bar{A}_0 for $i < i_r$, while for $i > i_r$, it weakly depends on \bar{A}_0 . Now let us focus on the relationship between i_g and i_r . If the convergence scale i_r is much smaller than i_g , the summation of the amplification rate of the noise, given by $\sum_1^{i_g} \lambda^S(i)$, depends little on the input. On the other hand, if i_r is larger than i_g , the downstream dynamics can strongly depend on the input. Hence, the conditions for the dependence on the input is represented [28] by

$$i_g \lesssim i_r \tag{27}$$

It may be interesting to compare the present boundary condition dependence with the initial condition dependence common to chaotic system, for example in a one-dimensional map. This comparison is summarized in Table 1.

6.3. Boundary condition dependence in the presence of time scale variation

In the present system with the time scale variation, it is also interesting to discuss the boundary condition dependence. Here, each site i has its own time scale T_i and spatial relaxation in the last section is discussed in terms of the time scale. The condition $i_g \lesssim i_r$ is then discussed in terms of the time scale.

Here we numerically check the condition Eq. (27). For larger τ , i_g is larger as shown in Fig. 4(b), because the convective instability exponent per element, characterized by $\Lambda^S(i)$, is smaller. On the other hand, for larger τ , i_r

Table 2

Boundary condition dependence in the open flow with the time scale variation

	Open flow with time scale variation
Each step	Time scale: T_i
Initial state	Fast scale property T_0, A, σ
Final state	Slow scale property $V(L), \bar{\Delta}(L) \gg T_0$
Instability	Convective instability $\kappa(\bar{f}_i) \simeq \Lambda^S(i) = \log V(i)/V(i-1)$
Dependence on initial state	Time scale of the boundary δT_0
Initial state sensitivity	$\sum_{i=1}^{i=i_g} \{ \kappa(\bar{f}_i) _{T_0+\delta T_0} - \kappa(\bar{f}_i) _{T_0} \}$
Condition	$i_g \lesssim i_r$

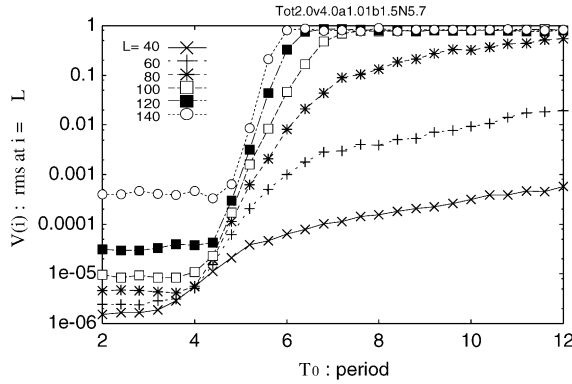


Fig. 11. The RMS of the slowest element $V(L)$ is plotted as a function of the period T_0 applied at the fastest element as $A \sin(2\pi t/T_0)$ with noise η (with the strength $\sigma = 10^{-3}A$). The marks correspond to a different set of (L, τ) as in Fig. 4. The dependence is sharper, and approaches threshold-type dependence, as τ is smaller.

is smaller (data are not shown). This is because the time scale multiplication is more difficult to occur due to larger time scale difference τ and the oscillation of $\Lambda(i)$ along the flow disappears only at the upper flow. From these tendencies and Eq. (27), it is expected that the boundary condition dependence in the slow dynamics is stronger as τ is smaller. This is demonstrated in Fig. 11 where the RMS of the slowest element is plotted as a function of the period T_0 , when the input $A \sin(2\pi t/T_0)$ with noise η is applied on the fastest element. There the boundary condition dependence is more strongly sensitive as τ is smaller. It also supports the validity of the condition Eq. (27). The boundary condition dependence for a system with the time scale variation is summarized in Table 2.

As described in Section 5.2, noise is necessary for the time scale multiplication. In the present simulation, noise is applied only at the fastest element $i = 1$. On the other hand, even if the Gaussian noise with a small amplitude is applied at the all elements, the above result is invariant. Hence, the present sensitive dependence on the input is both noise-induced and noise-tolerant.

6.4. Effect of the multiplication ratio

In Section 5.3, we have shown that the ratio of the single multiplication cycle is highly correlated with f_{\max}/f_{\min} . The multiplication is less frequent as f_{\max}/f_{\min} is larger. Then, according to the discussion in the last subsection, the relaxation length i_r is smaller, and the dependence on boundary condition is expected to be weaker. Here we discuss about such relationship of multiplication ratio with the sensitive dependence of slow dynamics on fast elements.

In Fig. 12 the RMS $V(L)$ of the slowest element L is plotted as a function of the period T_0 applied at the fastest element as $A \sin(2\pi t/T_0)$, together with the noise η , with the amplitude $\sigma = 10^{-1}A$. As v is smaller, the multiplication ratio, i.e., f_{\max}/f_{\min} , is smaller, the boundary condition dependence is more sensitive. Rather sharp threshold-type dependence is observed, then.

In conclusion, the dependence of slow dynamics on fast elements shows more sensitive as the multiplication ratio, correlated with f_{\max}/f_{\min} , is smaller.

7. Summary and discussion

7.1. Summary of the mechanism

In the present paper, we have reported translation of fast dynamics to slower dynamics by taking advantage of convective instability. The mechanism is explained by introducing the spatial instability exponent in the frequency

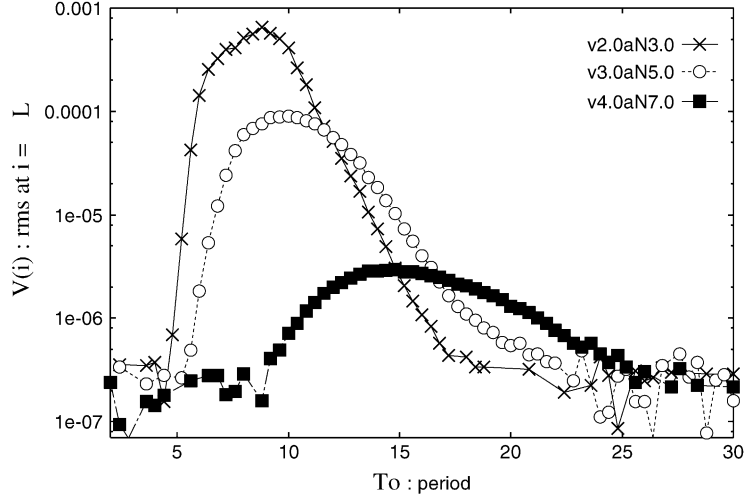


Fig. 12. The RMS of the slowest element $V(L)$ is plotted as a function of the period T_0 applied at the fastest element as $A \sin(2\pi t/T_0)$ with noise η (with the strength $\sigma = 10^{-1}A$). Here, the marks correspond to a different set of values of (v, k_2) that is adopted in Fig. 8(b)–(c). The ratio f_{\max}/f_{\min} is smaller as shown in Fig. 8(b)–(c). With the decrease of f_{\max}/f_{\min} , dependence of the downflow dynamics on T_0 is stronger.

space, given by $\kappa(\bar{f}_i)$, where $\bar{f}_i \equiv (\bar{\Delta}(i)/T_i)^{-1}$, instead of the spatial Lyapunov exponent λ^S . The phenomena and the mechanism we found are summarized as follows.

Time scale translation of the transmitted fluctuation with the use of convective instability is reported in Section 4. There the transmitted fluctuation is not only spatially amplified but also is made slower from the upstream to the downstream. This translation is realized by the time scale multiplication of the transmitted fluctuation, where the bifurcation to the motion with larger periods occurs successively. This mechanism is quantitatively expressed by the oscillation of $\Lambda(i) \simeq \kappa(\bar{f}_i)$ in Fig. 6 and the broader distribution of the fluctuation at the onset of the multiplication in Fig. 7(a). This time scale multiplication is found to occur when the following conditions are satisfied. First, the spatial instability exponent is positive only within a range of frequency $f_{\min} < f < f_{\max}$ as given by Eqs. (25) and (26). Second, non-periodicity of the transmitted fluctuation allows for a broad spectrum in the frequency. These conditions are satisfied at smaller τ , $\tau \lesssim 1.05$, i.e., $k_x \lesssim 2 \times 10^{-2}$ because of $\tau = \exp k_x$, in the present model as shown in Fig. 4(a).

Next, due to the convective instability with the time scale translation, the slow dynamics in the downstream are shown to sensitively depend on the fastest element in the upstream, as described in Section 6.1. It is realized by the modulation of the time scale multiplication process that depends on the dynamics of faster elements. By extending the boundary condition sensitivity introduced in [28,29] to include the change of time scale, the condition $i_g \lesssim i_r$ for the sensitivity is rewritten in Table 2. Accordingly the dependence is shown to be more sensitive as τ is smaller as shown in Fig. 11.

These mechanisms are maintained even if T_{total} is larger by fixing τ and making the system size L larger. It should also be noted that these mechanisms work even in an asymmetric reaction diffusion equation with time scale variation Eq. (6). The phenomena and the mechanisms are rather universal in a class of systems with spatially asymmetric coupling with the time scale change. As long as the conditions mentioned above are satisfied, the present phenomena are observed. These mechanisms and conditions are experimentally verifiable, because the measure of the convective instability, i.e., $\kappa(f)$ and $\Lambda(i)$ can be calculated from experimental time series data, as described in Eq. (17) and Appendix A.

7.2. Asymmetric diffusion from slow to fast element

In the subsection, we discuss about an open flow system where the time scale becomes faster as it goes to the downstream, in contrast to the system studied in the present paper. To be specific, we adopted $\tau < 1$ in Eq. (7).

For a NSS to propagate to the downstream with a faster time scale, the fluctuation is not only spatially amplified and transmitted, but also translated into a faster time scale, in contrast to the convective instability reported in Section 4. Then, instead of the time scale multiplication of the transmitted fluctuation around $\tilde{f}_i = f_{\max}$ in Section 4, the time scale division around $\tilde{f}_i = f_{\min}$ is necessary. Then, from the analogy of Eqs. (25) and (26) in Section 5.4, it is necessary for

$$\max_f \kappa(f) > 0, \quad \lim_{f \rightarrow \infty} \kappa(f) < 0, \quad \kappa(0) < 0 \quad (28)$$

We have studied several examples using Eq. (7) with $\tau < 1$. For some cases that satisfy with Eq. (28), the NSS is propagated with the time scale division of the transmitted fluctuation, and *sensitive* dependence of the downstream fast dynamics on the upstream slow dynamics is observed, similarly with Section 6. For some other cases, however, the NSS is not generated to downflow. For example, during the spatial amplification with the period division, refractory period of slower upstream elements is too long for the downstream faster elements, which may hinder the propagation of the NSS, even if Eq. (28) is satisfied.

If the time scale division works, the statistical properties of the fast elements can affect the slow dynamics in the open flow with $\tau > 1$. This is in contrast to the results in *symmetrically* coupled *chaotic* oscillators with power law time scale variation, where statistical properties of fast elements can affect the slow dynamics but that of the slow elements cannot affect the fast dynamics [10]. In this sense, the role of convective instability in the present case may be different from that of the chaotic instability in the previous study, though the appearance of the bifurcation cascade is common whenever the fast elements affect the slow dynamics. Further analysis is necessary for the case with $\tau > 1$, to discuss the condition for the transmission from slow to fast elements.

7.3. Relevance to a physical system

We discuss possible relevance of the present result to a physical systems, in particular, to memory effect in glassy systems, gel, granular materials and so forth [33].

As already mentioned in Section 3.2, in the avalanche behavior of a sand pile, it is observed that the particle flow on the surface is fast but the velocity gets much slower as the position is deeper from the surface [31]. Indeed, existence of such time scale variation distinguishes the granular flow from ordinary fluid flow. The flow at the horizontal direction along the surface, i.e., that of the granular flow in avalanche, is an open flow, while the system has a unidirectional coupling also along the vertical direction to the surface because granular particles are piled up on the vertical direction, and a flow at a deeper side is triggered to a faster flow at the surface. Since the time scale for the velocity increases along the vertical direction, the convective instability in this direction may lead to the time scale translation of the transmitted fluctuation reported in the present paper. It is then interesting to measure the development of the fluctuation and the void creation in the sand pile that may correspond to the time scale multiplication in the present paper. Then, through the convective instability, the slow creep motion in the inside of the sand pile can be sensitively dependent on the fast surface flow. This cascade transfer of flow could be studied in comparison with energy or inverse cascade in fluid turbulence.

History dependence of stress pattern in the sandpile on the way how granular particles are piled up is recently discovered [34]. The mechanism of the history dependence is discussed in terms of convective instability and the time scale variation from the surface to the inside [35]. Further study of the history dependence based on the time scale translation in the present paper may be relevant to understand the memory effect in such systems.

7.4. Relevance to biological system

Finally we give some remarks on the relevance of the present study to biological systems, which often involve multiple time scales. There, changes at a faster time scale sometimes affect the dynamics on slower time scales. In a biological system, this leads to various forms of ‘memory’. For example, cells can adapt to fast external changes, with some changes in their internal states [37]. In an intra-cellular signalling system, through cascade of reactions, environmental change is successively transferred to other chemicals, and then to the change of gene expression. Here each reaction has a different time scale, and the change of chemical concentrations at a downflow in the cascade may be slower [11]. Then, the mechanism presented in the paper provides a way how a fast external change is translated into a slower change of intra-cellular chemical states. Here, sensitive dependence on the external (boundary) condition is important for biological response.

In the above discussion, the suffix i of a_i in the present paper is regarded to correspond to a different chemical species (say kinase), and the unidirectional coupling is taken along the reaction network. It is also possible to consider more directly reaction-diffusion dynamics in a single cell, so that the suffix i denotes the real space. Due to the concentration gradient of some catalyzing chemicals, some parameters in the reaction equation vary accordingly (see [36], for a model for the embryonic development). When there is concentration gradient of the chemical C that has a property introduced in Section 3.2, it is possible that the concentration change near the membrane, i.e., the boundary condition of the upstream, can be fast, and the time scale is slower at the inside of the cell, i.e., at the downstream. With an external flow expressed as $v\partial b/\partial x$ in Eq. (5), this intra-cellular dynamics has an open-flow type coupling with the time scale variation. Then, a fast change near the membrane may crucially influence on the chemical state of the inside of the cell, and history dependence of the cell on the external environment may arise.

Another possible application of the results of the present paper will be a neural system, where fast changes in the input can be kept as memory over much longer time scales. The memory is believed to have different time scales, as often discussed in the regulation among short-term memories, long-term memories and learning [38,39]. Long-term potentiation of a single neuron involves cascade reactions, similarly to the MAP kinase cascade in the intra-cellular signalling system. The long-term potentiation appears as a response with a slower scale at the downstream of the cascade, depending on the environmental stimuli with a faster scale at the upstream of the cascade [12]. It is also interesting to note that the firing rate of neurons depends on area of the brain, and thus the time scale is changed as the external information is transferred. Thus, the mechanism in the present paper may shed new light on memory in brain.

Acknowledgement

A. Awazu, M. Matsuo, Y. Sato, T. Shibata and S. Ishihara for stimulating discussion and helpful comments.

Appendix A. The degree of the convective instability to periodic perturbation

We consider unidirectionally coupled ordinary differential equations as

$$\dot{\vec{A}}_i = \vec{G}(\vec{A}_i, \vec{A}_{i-1}) \quad (\text{A.1})$$

Here the stability analysis is calculated for $\vec{A}_i^* + \delta\vec{A}_i \equiv (a_* + \delta a_i, b_* + \delta b_i)$ as

$$\delta\dot{\vec{A}}_i = \left. \frac{\partial \vec{G}}{\partial \vec{A}_i} \right|_{\vec{A}_i=0} \delta\vec{A}_i + \left. \frac{\partial \vec{G}}{\partial \vec{A}_{i-1}} \right|_{\vec{A}_i=0} \delta\vec{A}_{i-1} \quad (\text{A.2})$$

where $\vec{A}_i^* \equiv (a_*, b_*)$ is a fixed point satisfied with $\dot{\vec{A}}_i = 0$ and $\delta\vec{A}_i \equiv (\delta a_i, \delta b_i)$. The Fourier transformation is introduced as

$$\vec{\Psi}_i(f) = \int \delta\vec{A}_i(t) e^{2\pi jft} dt \quad (\text{A.3})$$

where $\vec{\Psi}_i(f) \equiv (\psi_{a,i}(f), \psi_{b,i}(f))$. Then Eq. (A.2) is transformed as

$$2\pi jf \vec{\Psi}_i = \left. \frac{\partial \vec{G}}{\partial \vec{A}_i} \right|_{\dot{\vec{A}}_i=0} \vec{\Psi}_i + \left. \frac{\partial \vec{G}}{\partial \vec{A}_{i-1}} \right|_{\dot{\vec{A}}_i=0} \vec{\Psi}_{i-1} \quad (\text{A.4})$$

The spatial recursive equation for the frequency Fourier component is derived as

$$\left(- \left. \frac{\partial \vec{G}}{\partial \vec{A}_i} \right|_{\dot{\vec{A}}_i=0} + 2\pi jf \right) \vec{\Psi}_i = \left. \frac{\partial \vec{G}}{\partial \vec{A}_{i-1}} \right|_{\dot{\vec{A}}_i=0} \vec{\Psi}_{i-1} \quad (\text{A.5})$$

Accordingly, the degree of the convective instability to periodic perturbation with frequency f , i.e., $\kappa(f)$, is calculated from Eq. (A.5) by introducing the spatial recursive equation for the frequency Fourier component [24,25]. $\kappa(f)$ is given by logarithm of the transfer function from the spectra at the upstream to that at the downstream as

$$\kappa(f) = \log \frac{|\vec{\Psi}_i|}{|\vec{\Psi}_{i-1}|} \quad (\text{A.6})$$

Hence, we can experimentally calculate $\kappa(f)$ from power spectra of the fluctuation at the upstream and the downstream, when the strength of each fluctuation is not so large.

Appendix B. Calculation of the distribution of the fluctuation

The distance of each local maximum in the time evolution of x_i is defined as $\Delta_s(i)$ and measured as shown in Fig. B.1, s denotes the sample index. We construct the distribution from the collection of the samples $\Delta_s(i)$ for a long time.

The average and the root mean square of the distribution are calculated as

$$\begin{cases} \bar{\Delta}(i) \equiv \langle \Delta_s(i) \rangle_s \\ \delta\Delta(i) \equiv \sqrt{\langle \Delta_s(i)^2 \rangle_s - \bar{\Delta}(i)^2} \end{cases} \quad (\text{B.1})$$

$\langle \cdot \rangle_s$ means sample average for s . $\bar{\Delta}(i)$ denotes the average time scale of the fluctuation and $\delta\Delta(i)$ denotes the root mean square of the distribution.

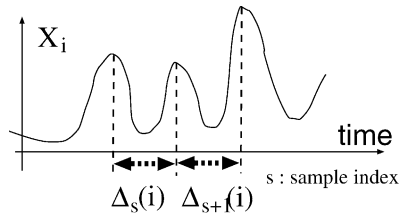


Fig. B.1. Schematic representation of the measurement of the distribution. $\Delta_s(i)$ is measured as the time interval of each local maximum of $x_i(t)$. s denotes sample index. By sampling $\Delta_s(i)$ for a long time, the distribution is constructed.

References

- [1] D.A. Fell, *Understanding the Control of Metabolism*, Portland Press, 1997 (Chapter 1).
- [2] M. Kumazawa, T. Ito, S. Yoshida (Eds.), *Decoding the Earth's Evolution*, Tokyo University Press, 2002 (in Japanese).
- [3] R.V. O'Neill, D.L. DeAngelis, J.B. Waide, T.F.H. Allen, *A Hierarchical Concept of Ecosystems*, Princeton University Press, 1986.
- [4] Y. Kakiuchi, T. Ueda, in preparation.
- [5] H.W. Pattee (Ed.), *Hierarchy Theory: The Challenge of Complex Systems*, George Braziller, 1973.
- [6] K. Kaneko, I. Tsuda, *Complex Systems: Chaos and Beyond*, Springer, 2000.
- [7] E.M. Lifshitz, L.P. Pitaevskii, *Physical Kinetics*, Pergamon, 1981.
- [8] P. Huerre, in: E. Tirapegui, D. Villaroel (Eds.), *Instabilities and Nonequilibrium Structures*, Reidel, 1987, pp. 141–177.
- [9] R.J. Deissler, *J. Stat. Phys.* 54 (1989) 1459–1488.
- [10] K. Fujimoto, K. Kaneko, *Phys. D* 180 (2003) 1–16;
K. Fujimoto, K. Kaneko, *Chaos* 13 (2003) 1041–1056.
- [11] B.D. Gomperts, I.M. Kramer, P.E.R. Tatham, *Signal Transduction*, Academic Press, 2002.
- [12] M.A. Lynch, *Physiol. Rev.* 84 (2004) 87–136.
- [13] K. Kaneko, *Phys. Lett.* 111A (1985) 321–325.
- [14] J.P. Crutchfield, K. Kaneko, in: B.L. Hao (Ed.), *Directions in Chaos*, World Scientific, 1987, 272–353.
- [15] I.S. Aranson, A.V. Gaponov-Grekhov, M.I. Rabinovich, *Phys. D* 33 (1988) 1–20.
- [16] F.H. Willeboordse, K. Kaneko, *Phys. D* 86 (1995) 428–455.
- [17] R.J. Deissler, *J. Stat. Phys.* 40 (1985) 371–395.
- [18] A.B. Rovinsky, M. Menzinger, *Phys. Rev. Lett.* 69 (1992) 1193.
- [19] R.A. Satnoianu, J.H. Merkin, S.K. Scott, *Phys. D* 124 (1998) 345–367.
- [20] R.J. Deissler, K. Kaneko, *Phys. Lett.* 119A (1987) 397–402.
- [21] K. Kaneko, *Phys. D* 23 (1986) 436–447.
- [22] D. Vergni, M. Falcioni, A. Vulpiani, *Phys. Rev. E* 56 (1997) 6170–6172.
- [23] G. Boffetta, M. Cencini, M. Falcioni, A. Vulpiani, *Phys. Rep.* 356 (2002) 367–474.
- [24] K. Konishi, H. Kokame, K. Hirata, *Phys. Lett.* 263 A (1999) 307–314;
K. Konishi, H. Kokame, K. Hirata, *Phys. Rev. E* 62 (2000) 6383–6387.
- [25] T. Shibata, *Phys. Rev. E* 69 (2004) 056218.
- [26] J. Liu, J.P. Gollub, *Phys. Rev. Lett.* 70 (1993) 2289–2292.
- [27] G. Nicolis, I. Prigogine, *Self-organization in Nonequilibrium Systems*, Wiley, 1977.
- [28] K. Fujimoto, K. Kaneko, *Phys. D* 129 (1999) 203.
- [29] K. Fujimoto, K. Kaneko, *Phys. Rev. E* 63 (2000) 036218.
- [30] W.H. Press, S.A. Teukolsky, W.T. Vetterling, *Numerical Recipes in C*, Cambridge University Press, 1993 (Chapter 17).
- [31] T. Komatsu, S. Inagaki, N. Nakagawa, S. Nasuno, *Phys. Rev. Lett.* 86 (2001) 1757.
- [32] M. Samoilov, A. Arkin, J. Ross, *J. Phys. Chem. A* 106 (2002) 10205–10221.
- [33] L. Cipelletti, L. Ramos, *Curr. Opin. Colloid Interface Sci.* 7 (2002) 228–234.
- [34] L. Vanel, D. Howell, D. Clark, R.P. Behringer, E. Clement, *Phys. Rev. E* 60 (1999) 5040;
J. Geng, E. Longhi, R.P. Behringer, D.W. Howell, *Phys. Rev. E* 64 (2001) 060301.
- [35] S. Ishihara, K. Kaneko, *J. Phys. Soc. Jpn.* 71 (2002) 2357–2360.
- [36] P. Borckmans, A. DeWit, G. Dewel, *Phys. A* 188 (1992) 137.
- [37] D.E. Koshland, *Science* 196 (1977) 1055–1063.
- [38] B.H. Morimoto, D.E. Koshland, *FASEB J.* 5 (1991) 2061–2067.
- [39] L.M. Kay, *Chaos* 13 (2003) 1057–1066.